

POLYTECHNIC UNIVERSITY OF TURIN

MASTER'S DEGREE IN ELECTRONIC ENGINEERING



**Politecnico  
di Torino**

# Vehicle Occupancy Detection

## Authors:

Matteo Caroleo *s344724*

Walter De Luca *s344245*

Edoardo Poggio *s348918*

Lorenzo Sgrò *s348963*

Turin — February 28, 2026

# 1 Introduction

The aim of this project is to implement a radar system based on the AWR1843 board, capable of detecting seat occupancy in a vehicle by using 4 receiving antennas.

The starting point was a code provided by our professors that performed range-only processing, without angular elaboration.

Our contribution consisted of modifying and extending the original project by introducing the computation of the range-azimuth map (through azimuth FFT) using EDMA (Enhanced Direct Memory Access) to handle data transfers in real time while using the same memory architecture given to comply with real-time specification.

## 2 Developed algorithm

In the original implementation, the real-time range-profile processing was limited to a subset of the available Rx channels.

In our modified version, the processing has been extended to exploit the full spatial information from the antenna array, enabling the computation of the range-azimuth map.

ADC capture samples are acquired from the two RX channels on which was applied range FFT to transform the time-domain chirp into the frequency domain, providing range information.

The FFT-range results are stored in memory L3 (RadarCube).

We began by updating the Rx antenna mask to enable the use of all four antennas, as required.

After that we added some modules that extended the project by introducing angular processing and data transfer optimization as reported in figure 1:

- **EDMA transfer from RadarCube to DataAzIn**

Since the RadarCube data are organized column-wise, we implemented two EDMA channels that are configured to read even or odd columns separately and to transpose them while transferring from RadarCube(L3) to DataAzIn(L1) memory.

In this way, the input for the angular FFT is prepared in the correct order without requiring additional DSP intervention.

- **Ping-Pong using EDMA**

To support real-time continuous streaming, the L1 memory is divided into two parts by following the ping-pong buffering paradigm.

While the DSP processes the data stored in one part of the L1 memory (FFT computation), the EDMA simultaneously fills the other part of the L1 memory with new data.

This mechanism enables real-time operation without stalling the pipeline.

On the architecture developed, the EDMA channel for even columns are written on the Ping buffer while the EDMA channel for odd columns in the Pong buffer.

- **Azimuth FFT**

For each range bin, we applied a spatial 64-point FFT (zero-padded up to 64 samples) across the RX channels to obtain the range-azimuth map.

The output of this step is stored in L2 memory (fftOut2D) and it is then moved with EDMA again in the next step.

- **EDMA transfer from fftOut2d to RangeAzMap**

The FFT results stored in fftOut2D (L2) are again divided into Ping and Pong regions in order to store results of fft while EDMA transfers the other portion of data in memory.

EDMA transfers these results to RangeAzMap (L3 memory) using Ping-Pong. While the fft computation stores its output data in a section of L2 memory the other section is transferred using another EDMA channel (regarding 'EDMA Output reconstruction').

This EDMA transfer is necessary because L2 is too small to contain all processed data.

- **Range-Azimuth Map (L3)**

After the last EDMA transfer we obtain the entire range-azimuth map stored in L3.

The magnitude of the angular FFT is computed offline (using a python script) to generate a 2D range-azimuth heatmap. The resulting map has dimensions  $256 \times 64$  bins.

This 2D heatmap represents the energy intensity (in dB) as a function of distance and angle, providing a clear visualization for occupant detection.

After the last step, it is possible to analyze the heatmaps to compare the empty seat vs occupied seat conditions.

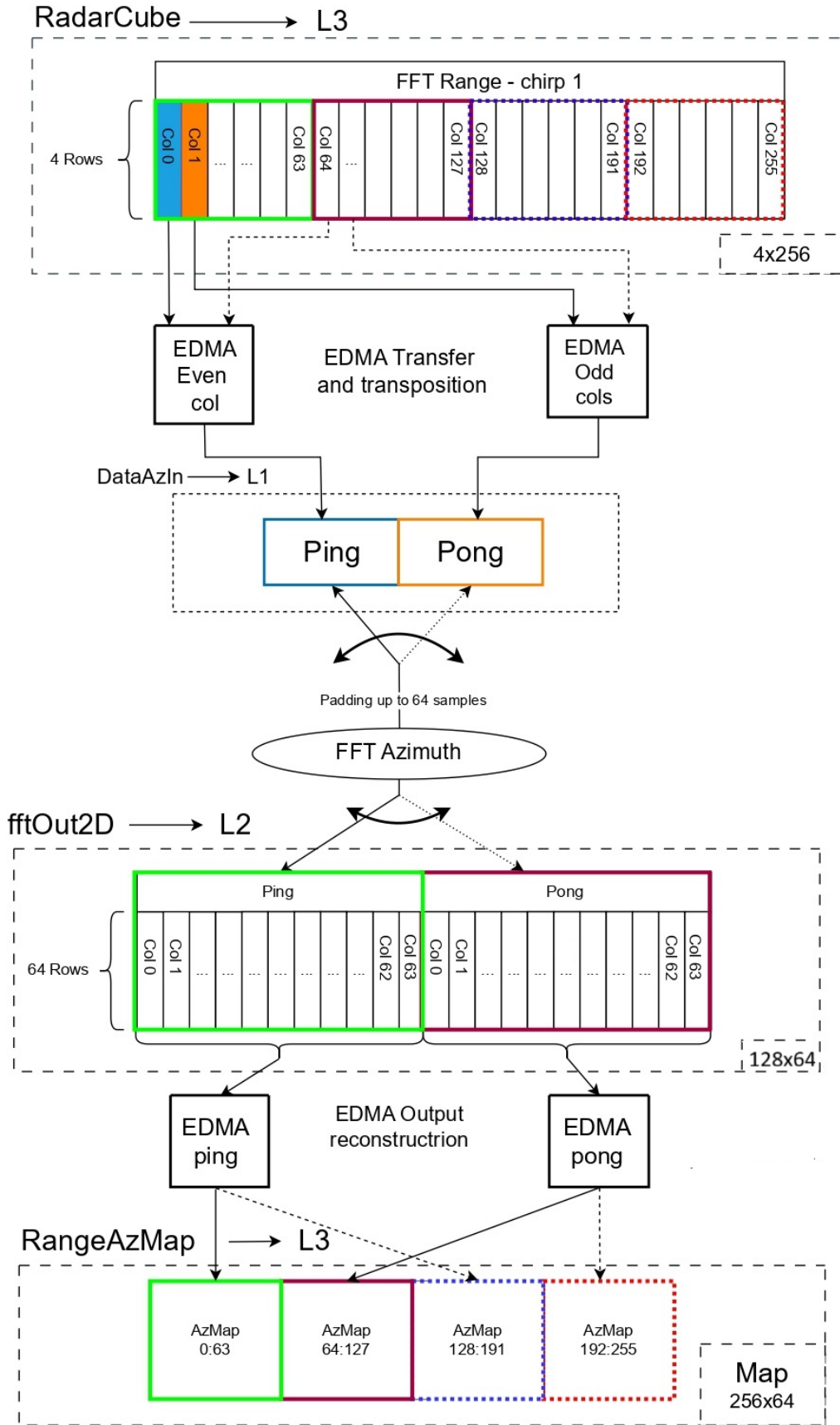


Figure 1: Schematic of the developed algorithm

### 3 Setup and calibration

We chose the open-field setup, shown in figure 2 and 3, to avoid cluttering from the background, even though ground cluttering is present.



Figure 2: setup



Figure 3: Homemade corner reflector used for calibration

The calibration process was carried out in order to eliminate the offset and to center the target by multiplying all values of each antenna with the respective complex coefficient. It was done using a homemade corner reflector as a precise reference.

The calibration started from the complex range matrix acquired(RangeAzMap) by placing the target centered at 2 meters and deriving the phase of all 4 receiving antennas over all ranges.

After finding the distance at which the target is located from the range profile produced by the radar the phase values at the target distance is obtained for every antenna.

To correctly calibrate the radar the phase of every receiving antenna must be brought to 0 at the target's distance.

To apply a phase shift to the acquired signal, each value can be multiplied by the complex conjugate corresponding to the opposite of the phase found at 0 degrees.

Inside the radar, this is then transformed in cartesian form as real and imaginary part.

For example, for the first antenna we found at the target range a phase of  $\phi$ : by using the notation  $e^{j\phi}$  we can compute the corresponding coefficients for compensation:  $e^{-j\phi} = 0.61 - 0.79j$ . After that, we update the stored values of first Rx antenna by multiplying them with newfound coefficient.

The graphs below show azimuth intensity at the distance of target before (figure 4) and after (figure 5) calibration. It can be seen that after calibration the main lobe is moved towards the center.

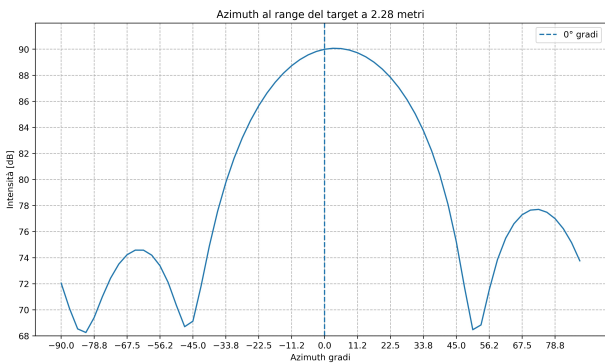


Figure 4: before calibration

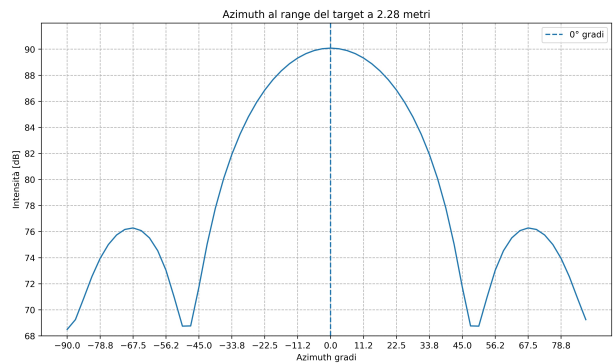


Figure 5: after calibration

## 4 Measures with corner reflector

The result of the test made with the centered corner reflector after calibration are found in figure 6 and in figure 7 both the main lobe and sidelobes are present.

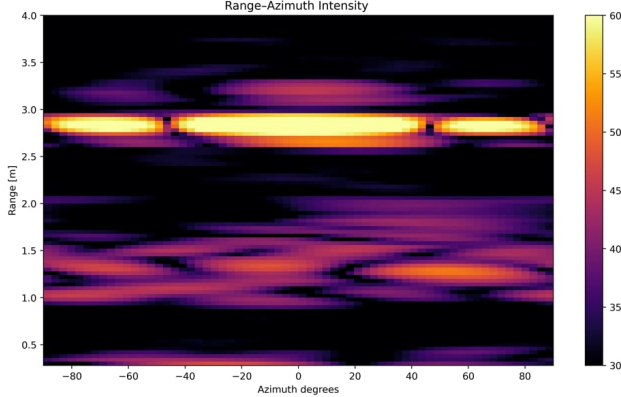


Figure 6: Azimuth Map with centered target at 2m

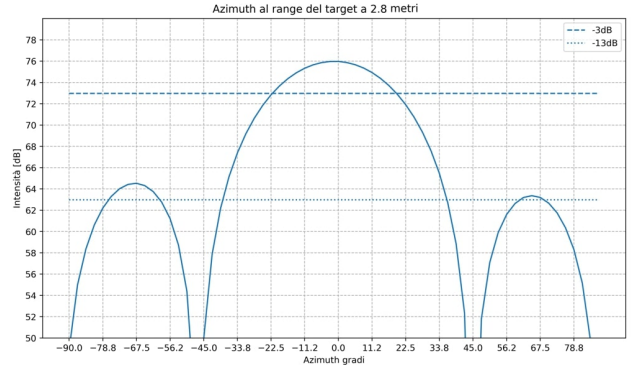


Figure 7: Intensity-azimuth graph at the target range

In Figure 8, the radar was physically rotated by  $90^\circ$ , which changed the angular scanning plane. As a consequence, the horizontal azimuthal dimension was replaced by the vertical elevation dimension, resulting in a Range–Elevation Map instead of a conventional Range–Azimuth Map.

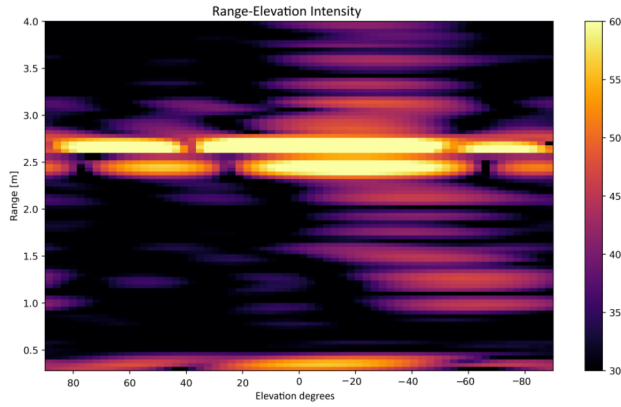


Figure 8: Elevation Map with centered target and rotated antenna at 2m

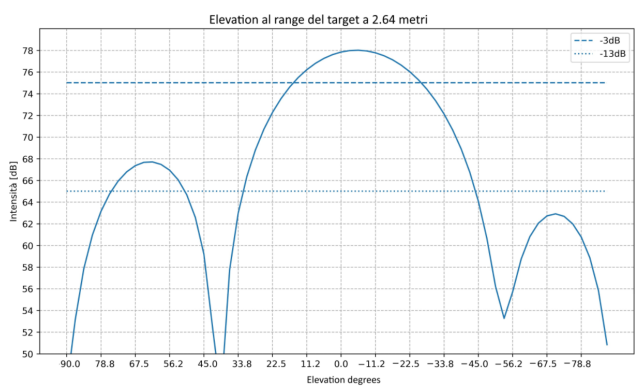


Figure 9: Intensity-elevation graph at the target range

In figure 10, a corner reflector was positioned to the left-hand side relative to the radar boresight, which produces a distinct return shifted accordingly along the angular axis. Conversely, in figure 12, the reflector was placed to the right-hand side, leading to a symmetric displacement of the response in the opposite angular direction.

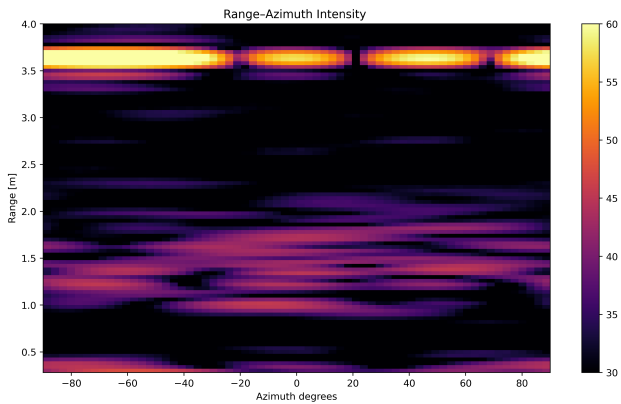


Figure 10: Azimuth Map with target on the left at 2m

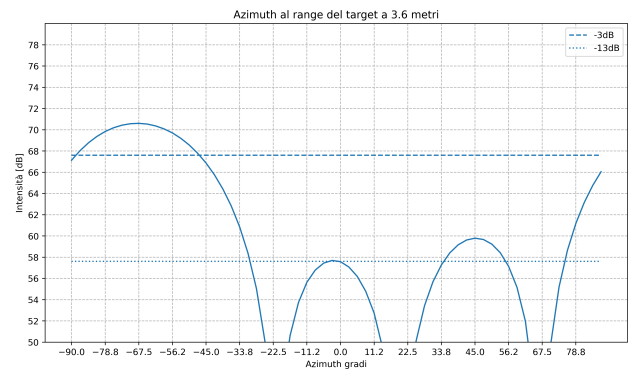


Figure 11: Intensity-azimuth graph at the target range located on the right side

In figure 12, a corner reflector was positioned to the right-hand side and is also reported in figure 13 his intensity-azimuth map at target distance.

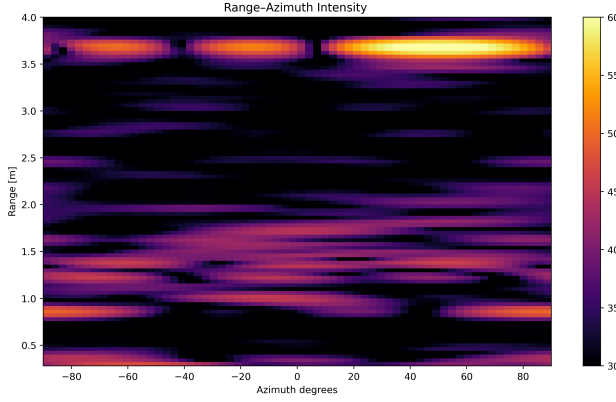


Figure 12: Azimuth Map with target on the right at 2m

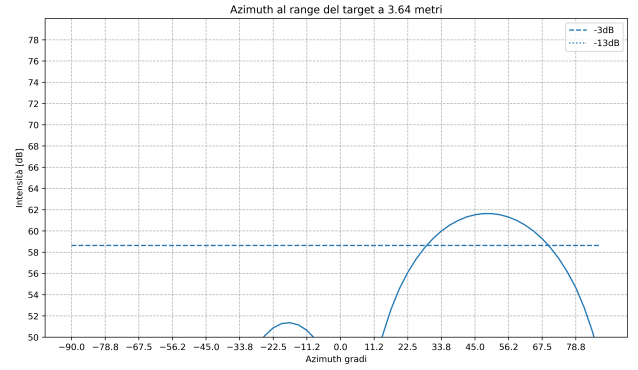


Figure 13: Intensity-azimuth graph at the target range located on the right side

#### 4.1 result of measures with corner reflector

From the azimuth intensity profile at about 2 meters (figure 7) the main lobe is visible at  $0^\circ$  with an amplitude of about 73 dB.

The sidelobes are 13 dB lower than the main lobe which indicates a ratio of  $\frac{1}{20}$ .

The displacement tests with the corner reflector placed on the left (Fig. 10) and on the right (Fig. 12) further confirms the functionality of the radar.

In both cases, the target response shifts symmetrically with respect to the antennas, demonstrating that the calibration holds also for off-centered targets.

Overall, the results show that:

- the calibration successfully removes antenna phase offsets and centers the main lobe;
- the measured main-to-sidelobe ratio is  $\approx 13$  dB;

## 5 Measures with human target

In the following images different measures are reported using human on a chair as the target, replacing the corner reflector.

For each target position we produced four images: heatmap and intensity graph as well for detection with and without the target, only the chair is in the correct position where the target will be located. We can compare the results obtained by radar with target located in the center of span in figure below. Comparing figures 15 and 17(target) with figures 14 and 16 we obtain a good distinction of two cases analyzed. The heatmaps show an higher peak at the range of target when the human is seated. To confirm this, the graph below displays that the peak of intensity at the target range with human is about 12 dB higher than the case without human, on the left.

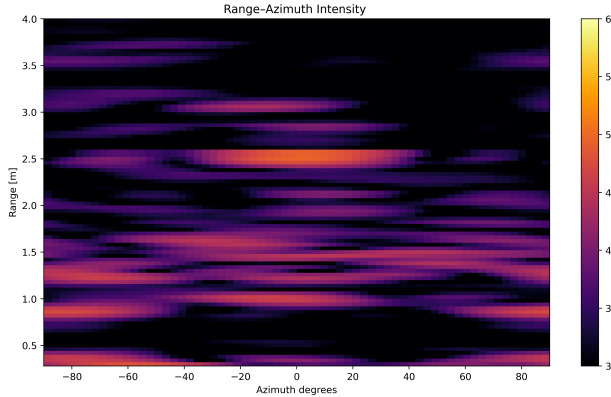


Figure 14: Azimuth Map without target

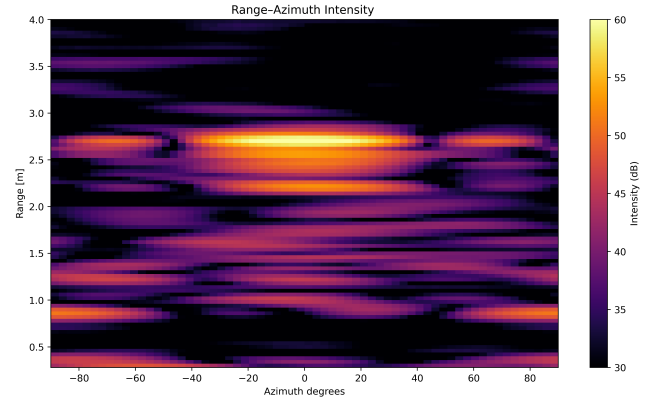


Figure 15: Azimuth Map with human as target

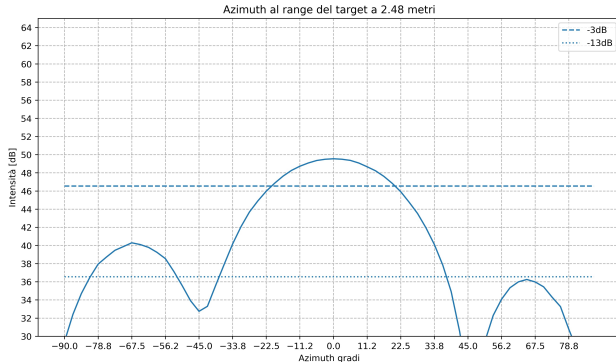


Figure 16: Intensity-azimuth graph at the target range without human target (only chair)

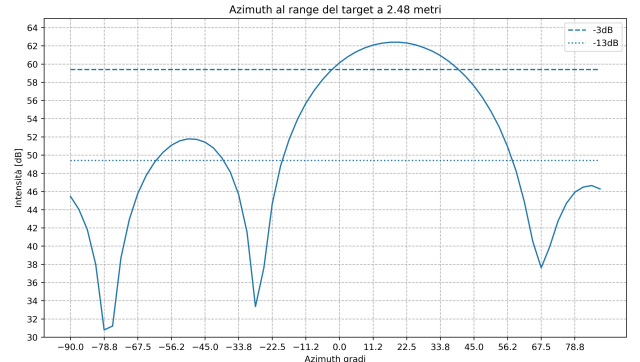


Figure 17: Intensity-azimuth graph at the target range with human target

On the next page the result of the azimuth and elevation with and without human are shown.

With the human target (figure 19) and the antenna rotated of 90° there is an increase of 3 dB with respect to the empty chair (figure 18). There is also an increase of the target's range, due to the position of the human body. The difference is clearer in figures 20 and 19 where range is fixed at the target position and the elevation intensity is shown.

With the human target (figure 15) on the right there is an increase of 12 dB with respect to the empty chair (figure 14). There is also an increase of the target's range like the previous measurement. The difference is clearer in figures 20 and 21 where range is fixed at the target position and the azimuth intensity is shown.

In the measurements taken, the -3dB width of the main lobe is always constant at about 40°, even without the target.

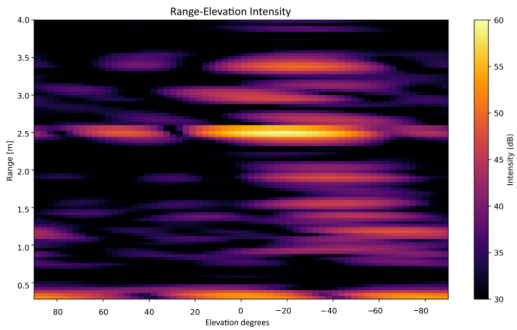


Figure 18: Elevation Map without target and rotated antenna

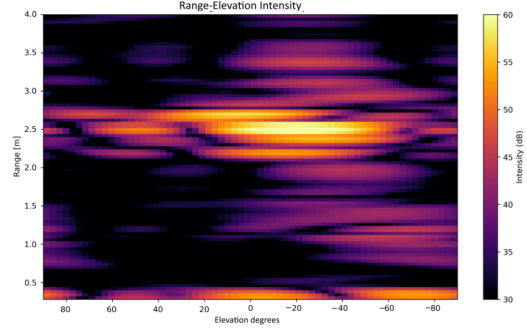


Figure 19: Elevation Map with human as target and rotated antenna

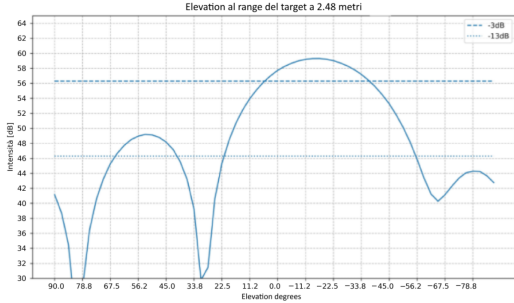


Figure 20: Intensity-elevation graph at the target range without human target (only chair) and rotated antenna

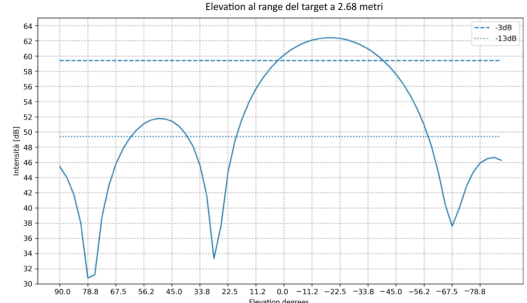


Figure 21: Intensity-elevation graph at the target range with human target and rotated antenna

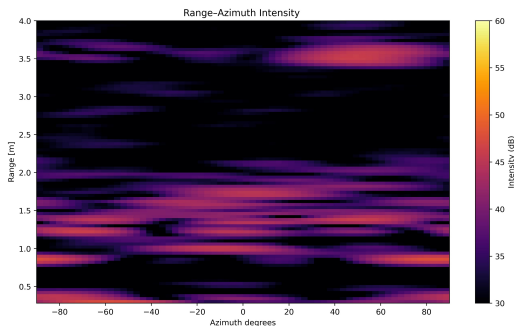


Figure 22: Azimuth map without human target (only chair located on the right side)

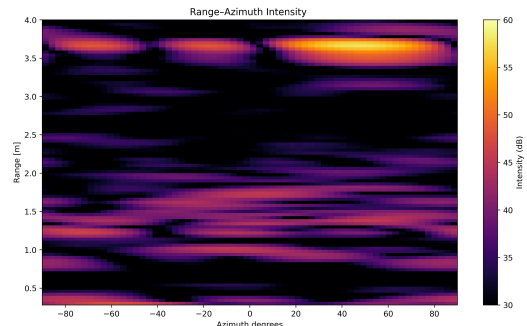


Figure 23: Azimuth Map with human as target on the right side

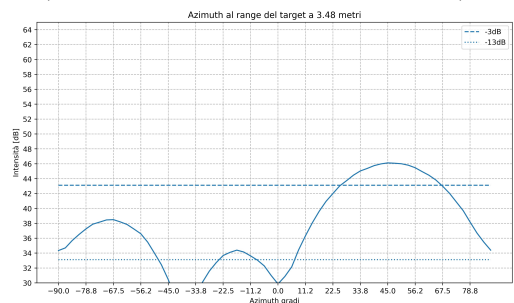


Figure 24: Intensity-azimuth graph at the target range without human target (only chair located on the right side)

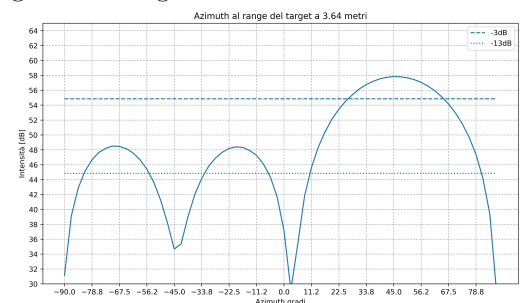


Figure 25: Intensity-azimuth graph at the target range with human target located on the right side

In conclusion, the range-azimuth measurements taken prove that the radar system developed is able to distinguish if a human is present on a chair. The range-elevation measurement has less of such difference of peak intensities, although present.